Atomistic simulation of ideal shear strength, point defects, and screw dislocations in bcc transition metals: Mo as a prototype

Wei Xu and John A. Moriarty
Lawrence Livermore National Laboratory, University of California, Livermore, California 94551
(Received 13 March 1996)

Using multi-ion interatomic potentials derived from first-principles generalized pseudopotential theory, we have studied ideal shear strength, point defects, and screw dislocations in the prototype bcc transition metal molybdenum (Mo). Many-body angular forces, which are important to the structural and mechanical properties of such central transition metals with partially filled *d* bands, are accounted for in the present theory through explicit three- and four-ion potentials. For the ideal shear strength of Mo, our computed results agree well with those predicted by full electronic-structure calculations. For point defects in Mo, our calculated vacancy-formation and activation energies are in excellent agreement with experimental results. The energetics of six self-interstitial configurations have also been investigated. The ⟨110⟩ split dumbbell interstitial is found to have the lowest formation energy, in agreement with the configuration found by x-ray diffuse scattering measurements. In ascending order, the sequence of energetically stable interstitials is predicted to be ⟨110⟩ split dumbbell, crowdion, ⟨111⟩ split dumbbell, tetrahedral site, ⟨001⟩ split dumbbell, and octahedral site. In addition, the migration paths for the ⟨110⟩ dumbbell self-interstitial have been studied. The migration energies are found to be 3–15 times higher than previous theoretical estimates obtained using simple radial-force Finnis-Sinclair potentials. Finally, the atomic structure and energetics of ⟨111⟩ screw dislocations in Mo have been investigated. We have found that the so-called ''easy'' core configuration has a lower formation energy than the ''hard'' one, consistent with previous theoretical studies. The former has a distinctive threefold symmetry with a spread out of the dislocation core along the ⟨112⟩ directions, an effect which is driven by the strong angular forces present in these metals. [S0163-1829(96)00434-1]

I. INTRODUCTION

It is very important to understand both deformation and defect properties of metals at the atomistic level in order to develop larger length-scale theories of their mechanical properties. For example, the ideal shear strength of a metal is an important parameter in modern theories of plasticity and fracture.[1] Likewise, accurate determination of the atomic core structure and energetics of isolated dislocations is believed to be crucial for the understanding of the low-temperature plasticity of bcc metals. Although the rapid improvement and development of experimental tools in recent years, e.g., the scanning tunneling microscope (STM), the field ion microscope (FIM), the high-resolution transmission electron microscope (HRTEM), etc., has significantly improved the prospects for directly observing the structures of crystal defects at the atomic level, many details of these structures remain beyond the scope of these tools. With the corresponding rapid development in high-performance computing capabilities and efficient numerical algorithms, however, atomistic simulations based on realistic physical models are becoming a powerful supplement to current experimental methods.

The accurate atomistic simulation of deformations and crystal defects in metals requires the use of quantum-mechanically based interatomic potentials which take into account the electronic structure of the metal in a meaningful and systematic way. Most calculations of point defects and dislocations in metals[2–5] have used radial-force empirical potentials, including both pair potentials and many-body ''glue'' models such as Finnis-Sinclair (FS) potentials[6] and embedded-atom-method (EAM) potentials.[7] It has been recognized, however, that this is not adequate in general for the central bcc transition metals, as discussed by Carlsson[8] and others. Accurate atomistic simulations of deformation and defect energetics in the bcc metals require the strong angular forces present in these materials which arise from multi-ion *d*-state interactions. In recent years, several interatomic potential schemes[9–12] based on tight-binding theory and explicitly containing angular-force contributions have been developed for bcc transition metals and applied successfully to study structural phase stability, surface properties, and point defects. At the same time, Moriarty[13] has derived multi-ion interatomic potentials for transition metals from first-principles generalized pseudopotential theory (GPT). For atomistic simulations on the bcc metals, a simplified model GPT or MGPT has been developed using canonical *d* bands and which produces entirely analytic three- and four-ion potentials.[14,15] In the case of molybdenum (Mo), MGPT potentials have been successfully applied to the cohesive, structural, elastic, vibrational, thermal, and melting properties of the bulk metal.[15] In this paper, we have applied the same MGPT potentials to study ideal shear strength, vacancy and self-interstitial formation and migration, and the structure of ⟨111⟩ screw dislocations in Mo. We intend these calculations to serve both as additional tests of the potentials in low-symmetry bulk geometries and as an important first step towards future studies on dislocation motion in bcc metal systems, including the calculation of the Peierls barrier and its environmental dependence.

To our knowledge, the problems of ideal shear strength,

self-interstitial migration, and screw-dislocation structure in bcc transition metals have not been treated previously with angular-force interatomic potentials. In this regard, the MGPT approach offers some clear advantages for the study of such deformation and defects properties by atomistic simulation, which can become very computationally intensive when realistic angular forces are included. As discussed previously,[13,14] the MGPT total energy functional containing three- and four-ion potentials has essentially the same d-band physics as a tight-binding total-energy expansion carried out to the fourth moment of the d-band density of states, which is the basis of the fourth-moment tight-binding (FMTB) interatomic potential schemes mentioned above.[9–12] However, the d-state matrix multiplication which is needed to evaluate these contributions is carried out *analytically*, once and for all, in the MGPT, rather than numerically ''on the fly'' as in the FMTB schemes. This leads to closed-form expressions for the three- and four-ion MGPT potentials which are highly flexible, computationally efficient, and provide very accurate forces. Consequently, we expect the MGPT approach to be somewhat faster than the FMTB schemes, although both are necessarily slow compared to short-ranged EAM or FS potentials. An explicit timing test here has shown, for example, that the present MGPT potentials are at least 40 times slower than simple FS potentials. Full optimization of the MGPT has not yet been achieved, however, and could provide significantly increased computational speed in the future.

This paper is organized as follows. In Sec. II, we first review the MGPT and discuss the specific potentials used in this work for Mo. Then in Sec. III we apply these potentials to the ideal shear strength of Mo. Our general simulation method to treat bulk defects is discussed in Sec. IV together with MGPT calculations of the formation and migration energies for an isolated vacancy and for various self-interstitials. In Sec. V, we then apply the same techniques to obtain the stable configuration and core structure of a $\langle 111 \rangle$ screw dislocation. Finally, our conclusions are given in Sec. VI.

II. MGPT INTERATOMIC POTENTIALS

The MGPT interatomic potentials used in this work are based on first-principles generalized pseudopotential theory.[13] A brief summary of the MGPT formalism as it applies here to Mo is given below; more complete details can be found in the papers by Moriarty.[14,15] The first-principles GPT provides a rigorous real-space expansion of the total energy of a bulk transition metal in the form

$$E_{\rm tot}(\mathbf{R}_1 \cdots \mathbf{R}_N) = N E_{\rm vol}(\Omega) + \frac{1}{2} {\sum_{i,j}}' v_2(ij) + \frac{1}{6} {\sum_{i,j,k}}' v_3(ijk) + \frac{1}{24} {\sum_{i,j,k,l}}' v_4(ijkl), \tag{1}$$

where $\mathbf{R}_1 \cdots \mathbf{R}_N$ denotes the positions on the N ions in the metal, Ω is the atomic volume, and the prime on each sum over ion positions excludes all self-interaction terms where two indices are equal. The leading volume term in this expansion, $E_{\rm vol}$, as well as the two-, three-, and four-ion interatomic potentials, v_2, v_3, and v_4, are volume dependent, but *structure independent* quantities and thus *transferable* to all bulk ion configurations. In the full GPT, however, the potentials are both long-ranged and nonanalytic functionals, so that the multidimensional potentials v_3 and v_4 cannot be readily tabulated for application purposes. In the MGPT, the potentials v_2, v_3, and v_4 are systematically approximated by introducing canonical d bands and other simplifications to achieve short-ranged, analytic forms, which can then be applied to both static and dynamic simulations. The radial-force, two-ion pair potential v_2 is obtained as a sum of simple-metal *sp*, hard-core overlap, and tight-binding-like d-state contributions:

$$v_2(r) = v_2^{sp}(r) + v_2^{\rm hc}(r) + v_2^{d}(r). \tag{2}$$

In Eq. (2) the simple-metal potential v_2^{sp} and the hard-core potential $v_2^{\rm hc}$ are retained directly from the first-principles GPT, while the d-state potential v_2^d is developed in the form

$$v_2^d = v_a [f(r)]^4 - v_b [f(r)]^2, \tag{3}$$

where $f(r)$ is the radial component of the tight-binding matrix element linking the two ions. For pure canonical d bands, $f(r) \propto r^{-5}$, but this has been generalized to include an r^{-p} radial dependence and a smooth Gaussian cutoff beyond a specified radius R_0:

$$f(r) = \begin{cases} (r_0/r)^p, & r < R_0, \\ (r_0/r)^p \exp[-\alpha(r/R_0 - 1)^2], & r > R_0. \end{cases} \tag{4}$$

Here $r_0 = 1.8 R_{\rm WS}$, with $R_{\rm WS}$ the Wigner-Seitz radius, and for Mo $R_0 = 2.15 R_{\rm WS}$, $\alpha = 125$, and $p = 4$. The latter values of R_0 and α ensure that $f(r)$ is negligible beyond second-neighbor distances in the bcc structure, while the value of p chosen is that most commensurate with the actual d bands for Mo.

The angular-force three- and four-ion potentials, v_3 and v_4, are obtained as the appropriate multi-ion generalizations of v_2^d. The potential v_3 is a three-dimensional function of the separation distances r_1, r_2, and r_3 linking three ions,

$$\begin{aligned} v_3(r_1, r_2, r_3) = {} & v_c f(r_1) f(r_2) f(r_3) L(\theta_1, \theta_2, \theta_3) \\ & + v_d \{ [f(r_1) f(r_2)]^2 P(\theta_3) \\ & + [f(r_2) f(r_3)]^2 P(\theta_1) \\ & + [f(r_3) f(r_1)]^2 P(\theta_2) \}, \end{aligned} \tag{5}$$

while the potential v_4 is a six-dimensional function of the six separation distances linking four ions,

$$\begin{aligned} & v_4(r_1, r_2, r_3, r_4, r_5, r_6) \\ & = v_e [f(r_1) f(r_2) f(r_4) f(r_5) M(\theta_1, \theta_2, \theta_3, \theta_4, \theta_5, \theta_6) \\ & \quad + f(r_3) f(r_2) f(r_6) f(r_5) M(\theta_7, \theta_8, \theta_9, \theta_{10}, \theta_5, \theta_{12}) \\ & \quad + f(r_1) f(r_6) f(r_4) f(r_3) M(\theta_{11}, \theta_{12}, \theta_5, \theta_6, \theta_3, \theta_4)]. \end{aligned} \tag{6}$$

The quantities L, P, and M in Eqs. (5) and (6) are universal angular functions which depend only on d symmetry and apply to all transition metals. These functions have exact analytic representations which are given in Ref. 14. The major computational effort comes in evaluating the four-ion an-

TABLE I. Bulk properties of bcc Mo. Quantities and units: cohesive energy E_{coh} and structural energies in eV; bulk modulus B and elastic constants C_{11}, C_{12}, C_{44}, and C' in Mbar; phonon frequencies L, T_1, T_2 in THz. All quantities are evaluated at the observed equilibrium atomic volume (105.1 a.u.); phonons are zone-boundary values except as indicated. Experimental data are room-temperature results.

	MGPT	Experiment	Band theory
E_{coh}	−9.03	−6.82 [a]	−6.19 [b]
B	2.64	2.64 [c]	2.64 [b]
C_{11}	4.66	4.66 [c]	4.40 [d]
C_{44}	1.10	1.10 [c]	1.39 [d]
C_{12}	1.63	1.63 [c]	1.62 [d]
C'	1.51	1.52 [c]	1.39 [d]
bcc-fcc	−0.41		−0.41 [b]
hcp-fcc	0.001		0.03 [b]
$L[\frac{3}{5}00]$	9.34	7.61 [e]	
$L[100]$	9.20	5.52 [e]	5.0 [f]
$L[110]$	8.11	8.14 [e]	
$T_1[110]$	6.13	5.73 [e]	5.8 [g]
$T_2[110]$	4.02	4.56 [e]	4.0 [g]
$L[\frac{2}{3}\frac{2}{3}\frac{2}{3}]$	6.32	6.16 [e]	6.1 [f]

[a]Reference 16.
[b]Reference 14.
[c]Reference 17.
[d]Reference 19.
[e]Reference 18.
[f]Reference 20.
[g]Reference 21.

gular function M, which depends on six independent angles and is necessarily complicated. While we have an exact and efficient representation of this function, full optimization has probably not yet been achieved and this is a goal for the future.

The five remaining d-state coefficients v_a, v_b, v_c, v_d, and v_e in Eqs. (3), (5), and (6) are material parameters which depend primarily on d-band filling and width. The potential terms with coefficients v_a, v_d, and v_e all contribute to the fourth moment of the d-band density of states, while those with coefficients v_b and v_c contribute to the second and third moments, respectively. In FMTB schemes the third-moment terms are usually neglected, while the fourth-moment terms are treated collectively and in fixed ratios. In the MGPT, on the other hand, both of these conditions are relaxed and all five coefficients are treated as independent parameters. This serves in part to compensate for the neglect of explicit d-state nonorthogonality and sp-d hybridization contributions to the potentials. The coefficients themselves may be constrained by any desired combination of theory and experiment. For the present Mo potentials, v_c has been fixed by theoretical considerations, while v_a, v_b, v_d, and v_e have been fit to bulk experimental data, as described in Ref. 15.

A few selected bulk properties of Mo calculated using these potentials are quoted in Table I and compared with both experimental data[16–18] and *ab initio* band-theory results.[14,19–21] The bulk modulus and the elastic constants agree with experiment by construction, as these quantities have been used in determining the potentials. The excellent agreement with band theory achieved for the bcc-fcc energy difference, on the other hand, is an important benchmark test of the MGPT. Phonons are also well described except near the [100] zone boundary, where a strong Kohn anomaly abnormally lowers the longitudinal $L[100]$ frequency.[20] In the MGPT, the calculation of the $L[100]$ phonon, as well as the hcp-fcc energy difference, suffers from the suppression of long-ranged d-state interactions both through Eq. (4) and by the neglect of higher-order potentials beyond v_4. Most other bulk properties investigated for Mo are well described by the MGPT potentials, however, including the pressure dependence of the bulk modulus and elastic constants, the Debye temperature, the Grüneisen parameter, and the high-temperature melting properties, as previously discussed.[15]

The use of volume-dependent bulk potentials in deformation and defect calculations, as in the present applications, raises the general question as to the importance of local volume changes in such calculations. While the GPT formalism has been extended to take these effects into account,[22] they have been shown to be small ($\sim$ 0.01 eV) in bcc metals for the test case of the vacancy formation energy. We believe, therefore, that these effects can be safely neglected in bulk calculations. Operationally, all of the present applications are carried out at a fixed total volume corresponding to the equilibrium atomic volume $\Omega_0 = 105.1$ a.u. of bcc Mo. The volume term E_{vol} is treated as a constant and the potentials v_2, v_3, and v_4 are applied at the atomic volume Ω_0.

III. IDEAL SHEAR STRENGTH

The calculation of the theoretical shear strength in bcc transition metals on a quantum-mechanical basis has previously been considered by Paxton *et al.*[23] These authors define the shear strength of the perfect crystal to be the ideal twin stress τ_c associated with the continuous homogeneous deformation of the crystal into itself via the observed twinning mode. This mode is specified by a shear direction $\boldsymbol{\eta}$ and a normal plane $\mathbf{K}$. For bcc crystals, $\boldsymbol{\eta} = [111]$ and $\mathbf{K}=(112)$. In the absence of tensile relaxation normal to $\mathbf{K}$, the atomic positions during the deformation can be very simply related to the amount of shear x. Specifically, the calculation may be carried out entirely using a single atom per unit cell and periodic boundary conditions, with the basis vectors of the sheared crystal given by

$$\mathbf{a}_1=\frac{1}{2}[\bar{1}11]+\frac{1}{6}\frac{x}{s}[\bar{1}\bar{1}\bar{1}], \tag{7a}$$

$$\mathbf{a}_2=\frac{1}{2}[\bar{1}11]+\frac{1}{6}\frac{x}{s}[\bar{1}\bar{1}\bar{1}], \tag{7b}$$

$$\mathbf{a}_3=\frac{1}{2}[1\bar{1}1]. \tag{7c}$$

At $x=s=1/\sqrt{2}$, one has $\mathbf{a}_1=(1/3)[\bar{2}12]$ and $\mathbf{a}_2=(1/3)[122]$, so that an exact bcc twin has been created. Along the twinning path one calculates a symmetric energy barrier,

$$W(x)=(E_{tot}[x]-E_{tot}[0])/N, \tag{8}$$

with a barrier height W_c at $x=s/2$. The corresponding stress is given by

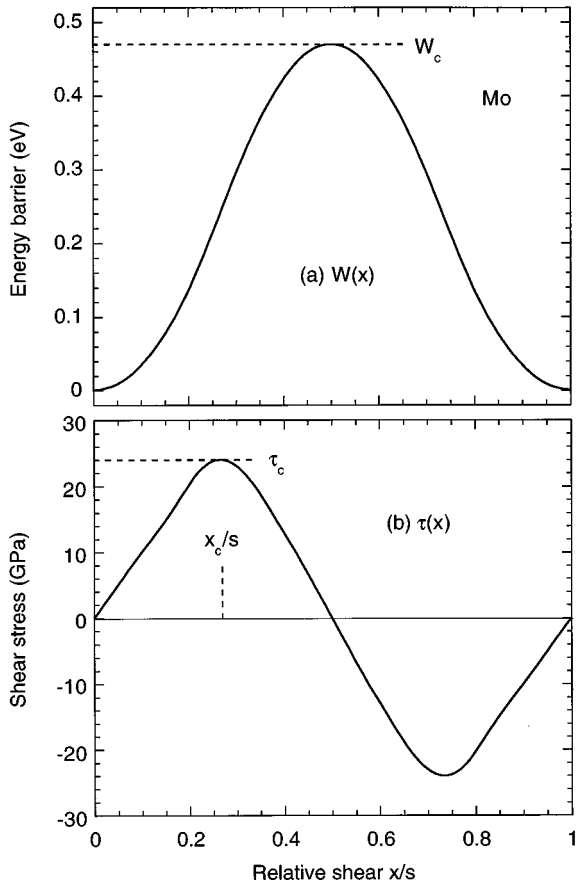

FIG. 1. Ideal shear strength in bcc Mo, as calculated with the present multi-ion MGPT interatomic potentials. (a) Energy barrier, $W(x)$; (b) shear stress, $\tau(x)$.

$$\tau(x)=\frac{1}{\Omega_0}\frac{dW(x)}{dx}. \tag{9}$$

The ideal shear strength is identified with the maximum calculated stress along the twinning path, $\tau_c=\tau(x_c)$, where x_c is the critical shear separating regimes of elastic and plastic deformation of the crystal. Paxton *et al.*[23] carried out this procedure for five bcc transition metals, including Mo, using a full-potential, linear-muffin-tin-orbital (FP-LMTO) electronic-structure method. These calculations were non-self-consistent, however, and employed the so-called Harris-Foulkes approximation, which they claim reproduces a full self-consistent calculation of τ_c in V to within 5%. This simplification also allowed these authors to consider relaxation effects in the form of a small applied tensile strain e ($0\leqslant e\leqslant 6\%$). The impact of relaxation was found to be small in all cases, however, and did not change τ_c by a significant amount. In the present work, therefore, we have considered only the unrelaxed $e=0$ case.

To test the present MGPT potentials for such large bulk deformations, we have applied the above $e=0$ scheme to Mo. We have calculated $W(x)$ at intervals of 0.01 over the full range $0\leqslant x\leqslant s$, and obtained $\tau(x)$ from numerical differentiation via Eq. (9). These results are plotted in Fig. 1. Calculated values of the barrier height W_c, critical stress τ_c, critical shear x_c, and corresponding shear modulus

TABLE II. Ideal theoretical shear strength in bcc metals, without tensile relaxation. Quantities and units: barrier height W_c in eV; critical shear x_c; critical stress τ_c and shear modulus μ_t in GPa.

	Mo FP-LMTO [b]	Mo MGPT	Mg [a] GPT	Na GPT
W_c	0.42	0.47	0.083	0.011
x_c/s	0.26	0.27	0.25	0.25
τ_c	19	23.7	3.52	0.20
μ_t	137 [c]	137.6	34.4	2.3
τ_c/μ_t	0.14	0.17	0.10	0.08

[a]Compressed metal: $\Omega/\Omega_0=0.723$, where bcc Mg is mechanically stable.
[b]Non-self-consistent calculations of Ref. 23.
[c]Assumed value.

$$\mu_t=(C_{11}-C_{12}+C_{44})/3 \tag{10}$$

are listed in Table II and compared with the results of Paxton *et al.*[23] The overall agreement is quite reasonable, although our value of τ_c is about 25% larger than theirs. Figure 2 illustrates the contributions of the multi-ion potentials to our calculated $W(x)$ and thereby the relative importance of the angular forces. While v_3 contributes almost nothing to $W(x)$ at any x, v_4 contributes about 50% at $x=x_c$ and about 33% to the total barrier height W_c.

It is also of interest to contrast our calculated results on Mo both with the predictions of the elementary Frenkel model of ideal shear strength and with corresponding results for simple bcc metals possessing no angular forces. In the Frenkel model, $\tau(x)$ is assumed to have the simple sinusoidal form[23]

$$\tau(x)=\frac{\mu_t s}{2\pi}\sin(2\pi x/s), \tag{11}$$

which yields $x_c/s=0.25$ and $\tau_c/\mu_t=s/2\pi\sim 0.1$. While the latter are quite respectable first approximations to bcc tran-

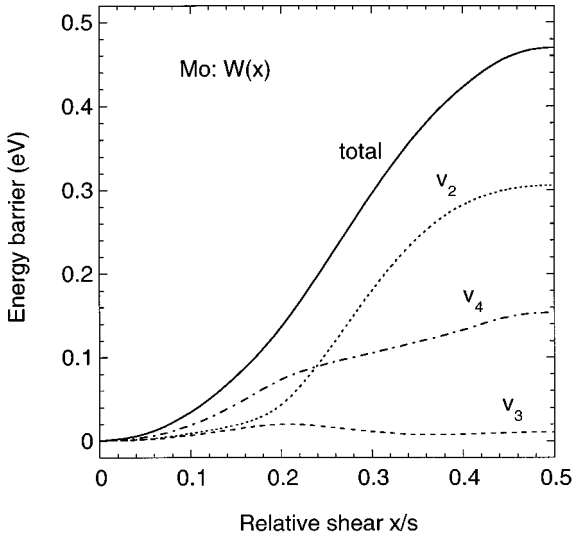

FIG. 2. Contributions to the shear-strength energy barrier in bcc Mo from the multi-ion MGPT potentials v_2, v_3, and v_4.

sition metal results, the actual behavior in these metals is somewhat more complex. As can be seen from Fig. 1, for example, our calculated $\tau(x)$ for Mo, while necessarily oscillatory, is clearly not a sine function. In addition, the calculated τ_c/μ_t are consistently higher than 0.1, with values in the range 0.12–0.17 for the cases studied by Paxton *et al.*[23] and a value of 0.17 here for Mo. This conclusion is reinforced when one considers simple bcc metals, which are well described by radial forces alone. Using first-principles GPT pair potentials for Mg (Ref. 24) and Na,[25] we have repeated the above calculations of ideal shear strength. The results are summarized and compared with those for Mo in Table II. In both metals the calculated $\tau(x)$ is much closer to a sine function and $\tau_c/\mu_t \simeq 0.1$, so that Frenkel behavior is indeed better approximated. At the same time, it is striking that while τ_c increases by 2 orders of magnitude between Na and Mo, τ_c/μ_t increases by only a factor of 2.

IV. POINT DEFECTS

The point defects studied here, i.e., the single isolated vacancy and the self-interstitial, are modeled within a large cubic simulation cell to which periodic boundary conditions are applied in all three directions. Fixed boundary conditions can also be used, but this requires considerably extra computer memory and usually produces slower convergence with respect to cell size, as we demonstrate below for the crowdion self-interstitial. The conjugate gradient method[26] is used to determine the stable structures through energy minimization. The formation energy for a point defects is defined as

$$E^f = E_{\rm tot}[N] - NE_{\rm coh}, \tag{12}$$

where $E_{\rm tot}[N]$ is the total energy of the simulated system, N is the number of atoms in the simulation cell including the defect, and $E_{\rm coh}$ is the cohesive energy (per atom) for bulk bcc Mo.

To calculate the migration energy barrier, we march one atom, which is either the interstitial atom or a nearest-neighbor atom in the vacancy case, from its equilibrium site towards a nearest-neighbor site or the vacancy site. During the migration process, we allow the migrating atom to relax in the plane perpendicular to the vector between its initial and final positions. This ensures finding the minimum (optimal) energy path for migration. Meanwhile, all other atoms are fully relaxed, except for one atom on the corner of the cell which is frozen to prevent a rigid shift of the simulation cell behind the ''marching'' atom. One stationary point (maximum) is found and it corresponds to the migrating atom sitting at a saddle point ($E_{\rm tot}=E_{\rm saddle}$) on the energy surface. The migration energy E^m is given by

$$E^m = E_{\rm saddle} - E_{\rm min}, \tag{13}$$

where $E_{\rm min}$ is the total energy of the defect at its equilibrium site.

A. Vacancy

Using MGPT interatomic potentials, we have calculated the formation and migration energies of a single isolated Mo vacancy. A simulation cell of size $5a\times5a\times5a$, where a is a lattice constant of Mo, was created with a total of 249 atoms plus one vacancy in the center. The calculation is carried out at zero temperature and constrained with a constant volume condition. In Table III we list the unrelaxed and relaxed vacancy formation energy, E_v^f that we obtain for Mo. Our relaxed formation energy of 2.9 eV is only about 4% lower than the unrelaxed value and in excellent agreement with experimental result measured by Maier *et al.*[27] Our unrelaxed and relaxed values also agree with the results obtained by Foiles[11] using a FMTB scheme. In both the MGPT and FMTB treatments, the unrelaxed formation energy was used as a constraining parameter in determining the potentials, so the consistency and agreement with experiment is not unexpected. For comparison, Harder and Bacon[4] obtained a value of 2.5 eV using the original Finnis-Sinclair potential, denoted as FS(1) in Table III, while the full tight-binding calculation of Ohta *et al.*[28] gave a much lower value of 0.9 eV. In order to check any size effect of the simulation cell on our result, a larger cell with 685 total atoms has also been used. We found that the formation energy so obtained is almost identical to that of the 249-atom cell ($<1\%$ difference).

TABLE III. Single vacancy formation energy E_v^f, migration energy E_v^m, and activation energy Q_v for Mo, in eV.

	MGPT	FMTB [a]	FS(1) [b]	Experiment [c]
E_v^f(unrelaxed)	3.0	3.0		
E_v^f(relaxed)	2.9	2.9	2.5	3.0 ($\pm$ 0.3)
E_v^m	1.6	1.9	1.3	
Q_v	4.5	4.8	3.9	4.5 ($\pm$ 0.3)

[a]Reference 11.
[b]Reference 4.
[c]Reference 27.

In the calculation of the vacancy migration energy, E_v^m, we constrained the migrating atom, a nearest neighbor of the vacancy, to lie on a plane which is perpendicular to the migration path along $\langle 111\rangle$. As indicated in Table III, our calculated migration energy for Mo is 1.6 eV, as compared with 1.9 eV obtained by Foiles[11] with FMTB potentials and 1.3 eV obtained by Harder and Bacon[4] with FS(1). Experimentally, only the activation energy, Q_v, which is the sum of vacancy formation and migration energies, can be measured. Using our calculated values of E_v^f and E_v^m we find that the activation energy Q_v is 4.5 eV for Mo, in excellent agreement with the measured result, and somewhat better than the values of 4.8 and 3.9 eV obtained by Foiles[11] and by Harder and Bacon,[4] respectively.

TABLE IV. Percentage displacements of nearest-neighbor (NN) shells to a relaxed Mo vacancy, as obtained in the present MGPT calculations.

Shell	Unrelaxed	Relaxed	%
First NN	0.866025a	0.850189a	-1.83
Second NN	1.000000a	1.004617a	$+0.46$
Third NN	1.414214a	1.415590a	$+0.10$
Fourth NN	1.658312a	1.657589a	-0.04
Fifth NN	1.732051a	1.724861a	-0.42
Sixth NN	2.000000a	2.000256a	$+0.01$
Seventh NN	2.179449a	2.178924a	-0.02

TABLE V. Self-interstitial formation energy E_i^f of six interstitial sites for Mo, in eV.

Interstitial configurtation	Position in bcc lattice	E_i^f MGPT	E_i^f FS(1) [a]
$\langle 110\rangle$ split dumbbell	$\pm(0.26,0.26,0.00)a$	10.9	7.0
Crowdion	$(0.25,0.25,0.25)a$	13.9	7.2
$\langle 111\rangle$ split dumbbell	$\pm(0.22,0.22,-0.22)a$	14.2	7.3
Tetrahedral	$(0.50,0.25,0.00)a$	14.9	7.6
$\langle 001\rangle$ split dumbbell	$\pm(0.38,0.00,0.00)a$	16.3	7.2
Octahedral	$(0.50,0.50,0.00)a$	17.5	7.6

[a]Reference 4.

While the effects of relaxation are small, we have found that the displacement of atoms around the relaxed vacancy follows a clear oscillatory pattern, with an inward contraction of the first-neighbor shell by about 1.8%. Table IV indicates the change in radius of the first seven nearest-neighbor (NN) shells to the vacancy site. In particular, the displacements follow contraction, expansion, expansion, contraction, contraction, expansion, and contraction. A qualitatively similar relaxation pattern for the first two shells was obtained by Matthai and Bacon[3] with the FS(1) potential. The tight-binding calculation of Ohta *et al.*,[28] on the other hand, showed little or no relaxation of the first shell and an inward relaxation of the outer shells.

B. Self-interstitials

We have carried out MGPT calculations on Mo self-interstitials for the various possible high-symmetry positions in a bcc structure. Six different configurations have been considered which include octahedral, tetrahedral, and crowdion sites, and split dumbbell sites along the $\langle 110\rangle$, $\langle 001\rangle$, and $\langle 111\rangle$ directions. These interstitials are shown in Fig. 3. All six configurations are metastable and the calculated equilibrium positions are given in Table V. Due to the large strain fields generated by such interstitial defects, it is important to check the convergence of the formation energy, E_i^f, with respect to simulation cell size in constant volume calculations. We have considered four cells ($6a\times6a\times6a$ with 432 atoms, $7a\times7a\times7a$ with 686 atoms, $8a\times8a\times8a$ with 1024 atoms and $9a\times9a\times9a$ with 1458 atoms) to calculate the formation energy. Table VI shows the convergence of E_i^f for the crowdion self-interstitial with respect to the size of the simulation cell, using both periodic boundary conditions and fixed boundary conditions. In the latter case, the system must include a large surrounding outer region, where the atomic positions are fixed at their bulk bcc values, in addition to the inner simulation region, where the atomic positions are fully relaxed. Table VI shows the calculated formation energy for four simulation cells with different-sized inner regions. Although the two methods indeed appear to be uniformly converging toward the same result, for any given cell size we obtain a higher, and hence less converged, formation energy with fixed boundary conditions than with periodic boundary conditions. Another major drawback in using fixed boundary conditions is that they require a very large outer region to satisfy the interatomic-potential cutoff ($\sim 2.1a$) for the inner-region boundary atoms. For example, a simulation cell with 1458 atoms in the inner region still needs an additional 4000 atoms in the outer region to satisfy the cutoff. This consequently slows down the calculation due to large additional computer memory required.

Based on this detailed test, we have chosen a 1024-atom cell to use in all our remaining calculations with periodic boundary conditions. The resulting formation energies for the six interstitial configurations are listed in Table V. We find the $\langle 110\rangle$ split dumbbell to have the lowest formation energy, $E_i^f = 10.9$ eV at $\pm(0.26,\ 0.26,\ 0.0)a$, in agreement with the configuration found by x-ray diffuse scattering measurements.[29] In ascending order, the sequence of energetically stable interstitials is $\langle 110\rangle$ split dumbbell, crowdion, $\langle 111\rangle$ split dumbbell, tetrahedral site, $\langle 001\rangle$ split dumbbell, and octahedral site. Table V also lists the results on self-interstitial formation energies in Mo calculated by Harder and Bacon[4] using the original Finnis-Sinclair potential, FS(1). Obviously, MGPT yields much higher values than FS(1), and this is a direct reflection of the strong angular forces present in the former potentials, which disfavor non-bcc angles. On the other hand, for the $\langle 110\rangle$ split dumbbell, Foiles[11] obtained a formation energy of only 6.2 eV with his FMTB scheme, which is actually 0.8 eV *lower* than the FS(1) result. This emphasizes that interstitial energies are sensitive to the short-range details of the interatomic potentials as well as to the angular forces.

An asymmetric metastable configuration at $\pm(0.3182,\ 0.1958,\ 0.0182)a$, which is rotated from the $\langle 110\rangle$ dumbbell position $\pm(0.26,\ 0.26,\ 0.0)a$, has been reported previously with the lowest formation energy by Thetford[30] using a modified Finnis-Sinclair potential, FS(2). To check this so-called bent configuration, we also broke the symmetry of the $\langle 110\rangle$ dumbbell and relaxed the structure. However, our calculations revealed that the bent interstitial is an unstable configuration which will eventually return to the original $\langle 110\rangle$ dumbbell position.

TABLE VI. Convergence of crowdion interstitial formation energy, in eV, using both periodic boundary conditions (PBC) and fixed boundary conditions (FBC). Here the cell size for FBC refers to the inner region, where all atomic positions are fully relaxed, as in the case of PBC.

Cell size	Number of atoms	E_i^f(crowdion) PBC	E_i^f(crowdion) FBC
$6a\times6a\times6a$	432	14.04	14.26
$7a\times7a\times7a$	686	13.93	14.11
$8a\times8a\times8a$	1024	13.88	14.03
$9a\times9a\times9a$	1458	13.85	13.97

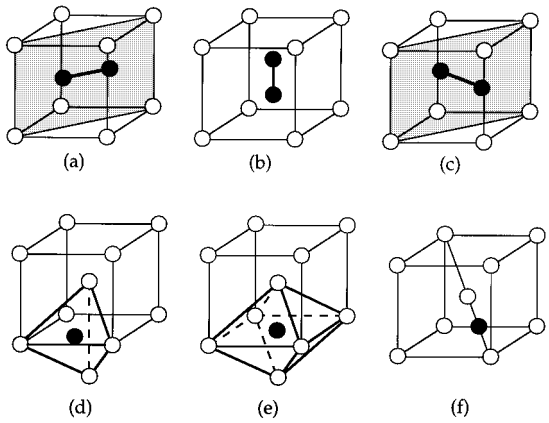

FIG. 3. High-symmetry interstitial configurations in bcc Mo: (a) ⟨110⟩ split dumbbell, (b) ⟨001⟩ split dumbbell, (c) ⟨111⟩ split dumbbell, (d) tetrahedral site, (e) octahedral site, and (f) crowdion site.

We have studied three migration mechanisms for a ⟨110⟩ split dumbbell interstitial migrating along ⟨111⟩ directions (Fig. 4). Paths *A* and *B* involve migrations of the dumbbell center to one of its nearest-neighbor sites along ⟨111⟩ with a jump length $\sqrt{3}/2a$. The difference between paths *A* and *B* is that the orientation of the dumbbell will rotate to another ⟨110⟩ direction in path *B* (jump plus rotation mechanism), while it will remain the same in path *A* (parallel jump mechanism). In path *C* the dumbbell will not change its orientation, only the center will make a double jump along ⟨111⟩. As shown in Table VII, we find that path *B* easily possesses the lowest migration energy barrier in Mo, 0.76 eV, as compared with values over 2 eV for paths *A* and *C*. At the same time, the magnitudes of the MGPT migration energies are 3–15 times higher than previous theoretical estimates[4,5] obtained using the simple radial-force Finnis-Sinclair potentials for Mo, FS(1), and FS(2). This again reveals the influence of the strong angular forces in the MGPT potentials.

V. ⟨111⟩ SCREW DISLOCATIONS

In calculating the structure of a ⟨111⟩ screw dislocation, we construct a slab with the *z* direction parallel to the Burgers vector **b**, which is along ⟨111⟩. The *x* and *y* directions are chosen along ⟨112⟩ and ⟨110⟩, respectively (see Fig. 5). Periodic boundary conditions are applied in the *z* direction only, in order to simulate an infinite straight screw dislocation. In the *x* and *y* directions, we use fixed boundary conditions. In doing so, we must as above divide the system into two regions: an inner region and an outer region. The dislocation core is contained in the inner region, where atomic positions are fully relaxed. The outer region surrounds the inner region and in it atomic positions are fixed according to the initial displacements generated by anisotropic elasticity theory.[31] Simulation cells of different total sizes ranging from 600 atoms up to 2160 atoms have been considered in the calculation. Due to the large distortion caused by the dislocation, however, a large simulation cell is required to yield a stable core. Except as indicated, we here present results obtained from a 1946-atom system with 1074 atoms in the inner region.

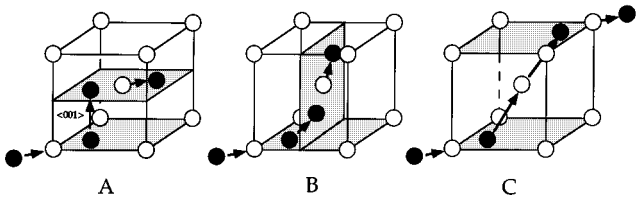

FIG. 4. Schematic of self-migration paths (*A*, *B*, and *C*) for the ⟨110⟩ split dumbbell interstitial.

TABLE VII. Migration energy E_i^m for the ⟨110⟩ split dumbbell interstitial for Mo, in eV.

Path of migration	E_i^m MGPT	FS(1) [a]	FS(2) [b]
A: parallel jump	2.52	0.18	0.25
B: jump + rotation	0.76	0.16	0.23
C: two parallel jumps	2.12	0.24	

[a]Reference 4.
[b]Reference 5.

Two stable dislocation-core configurations in bcc Mo have been investigated in detail, each with the core center located at the gravitational center of a triangle surrounded by three ⟨111⟩ atom rows. The first one of these is the so-called ''hard''-core ⟨111⟩ screw dislocation with the Burgers vector **b** in the positive *z* direction. In this configuration, the bulk ordering of the three neighboring ⟨111⟩ atom rows

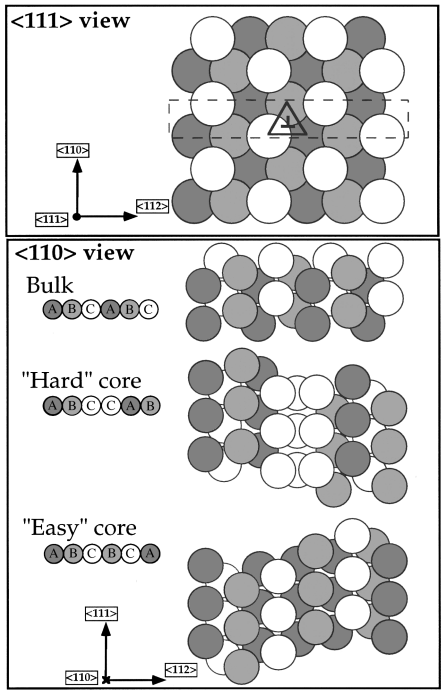

FIG. 5. Top view (⟨111⟩) and side view (⟨110⟩) of the ⟨111⟩ screw dislocations in Mo. Side views are only two rows of atoms which contain the dislocation center (dashed-line region in the top view). The stacking sequences of one {110} plane for the bulk bcc structure and for the ''hard''- and ''easy''-core dislocations are shown in the side view.

which are closest to the core center is destroyed and atoms from those three rows are aligned into the same {111} planes, as shown in Fig. 5. As also shown in that figure, the stacking sequence of atom rows for bulk bcc Mo is $ABCABC\ldots$ along $\langle 112\rangle$ in a {110} plane, but this sequence changes to $ABCCAB\ldots$ for the ''hard''-core dislocation. The second configuration we have considered is the so-called ''easy'' core $\langle 111\rangle$ screw dislocation. This configuration has its Burgers vector in the opposite direction to the ''hard'' one, with both dislocation-core centers located on the same site. The bulk ordering of the three atom rows surrounding the core center is preserved but reversed in sense, leading to a stacking sequence of $ABCBCA\ldots$ along $\langle 112\rangle$ in a {110} plane, as shown in Fig. 5. Using the angular-force MGPT potentials, we have found that the ''easy'' core configuration in Mo has a lower formation energy than the ''hard'' one, which is consistent with previous theoretical studies using empirical pair potentials[2]. We have also found that the inner-region atoms are relaxed in all three directions, especially the x and y directions. The magnitude of the largest in-plane relaxation is about one-tenth of the Burgers vector. At the same time, the forces on the inner boundary atoms located between the inner and outer regions are negligible with magnitudes $\sim 10^{-3}$ eV/Å. In addition, we have considered displaced locations for the dislocation-core center along a $\langle 111\rangle$ atom row and in the surrounding vicinity. We have found that these displaced centers all produce dislocation configurations with higher formation energies. This indicates that the energetically favored structure for a $\langle 111\rangle$ screw dislocation is indeed one with its center located at the assumed gravitational center of a triangle surrounded by three $\langle 111\rangle$ atom rows.

Kimura *et al.*[32] have also reported full tight-binding calculations on $\langle 111\rangle$ screw dislocation-core structures in Mo. Two kinds of core configurations have been calculated. The first they denote as the nondegenerate unpolarized core. This dislocation is introduced by displacing atoms according to isotropic linear elasticity theory. Unfortunately, they did not distinguish their dislocation cores with regard to the ''hard'' or ''easy'' direction, i.e., whether the Burgers vector **b** is in the positive z or negative z direction, as discussed above. Their nondegenerate unpolarized core, however, was calculated to be stable and its detailed differential displacement field appears to correspond to our ''hard-core'' configuration. The second configuration they have considered is denoted as a doubly degenerate polarized core. This dislocation is constructed from the nondegenerate core by uniformly displacing three neighboring $\langle 111\rangle$ atom rows which are closest to the core center in the $+z$ direction by an amount Δz_1 and three second-nearest-neighboring $\langle 111\rangle$ atom rows of the core in the $-z$ direction by an amount Δz_2. Thus the doubly degenerate core possesses a similar stacking sequence to the nondegenerate core. Using assumed values of Δz_1 and Δz_2, they calculated the total energy of a doubly degenerate core and concluded it was an energetically unfavorable structure. In order to make a more complete comparison, we also constructed such doubly degenerate dislocations from our relaxed ''hard'' and ''easy'' cores, respectively. Our final results indicate the doubly degenerate cores are not stable structures and will eventually relax to their initial ''hard'' or ''easy'' configurations, in agreement with the tight-binding calculation.

In the general elasticity theory, the formation energy E^f of a dislocation in a cubic crystal is a linear function of $\ln(R/R_c)$, where R is the outer cutoff radius of a cylinder which contains the dislocation core at its center. The inner cutoff radius R_c is defined as the core radius. We note the formation energy E^f includes two parts: (1) the core energy stored inside the R_c, $E^f_{\rm core}$; plus (2) the energy stored in the region between R_c and R, $E^f_{\rm outer}$. For a $\langle 111\rangle$ screw dislocation in bcc Mo, anisotropic elasticity theory[31] yields the result

$$E^f = E^f_{\rm outer} + E^f_{\rm core} = \frac{K_s b^3}{4\pi}\ln(R/R_c) + E^f_{\rm core}, \qquad (14)$$

where K_s is related to the anisotropic shear modulus and can be written as

$$K_s = [S_{11}/S_{44}(S_{11}S_{44} - S_{15}^2)]^{1/2}. \qquad (15)$$

The S_{11}, S_{44}, and S_{15} are modified elastic compliances which are related to the standard elastic compliances s_{11}, s_{44}, and s_{15} and to the elastic constants of the cubic crystal. The details of S_{11}, S_{44}, and S_{15} can be found in Ref. 31. Using the MGPT values of the three elastic constants C_{11}, C_{12}, and C_{44} listed in Table I, we calculate $K_s = 1.357$ Mbar. To make a quantitative correspondence between Eq. (14) and our atomistic calculations, we have first tentatively set $R_c = 2b$, the approximate expected value of the core radius. We have then computed the MGPT formation energy E^f of the ''easy''-core $\langle 111\rangle$ screw dislocation as a function of the radius R of a cylinder which contains the dislocation core. We define this cylinder to coincide with the inner region of our simulation cell, so that the axis of the cylinder passes through the dislocation core center. By increasing the radius R, we have thereby generated a plot of E^f/b vs $\ln(R/2b)$, as

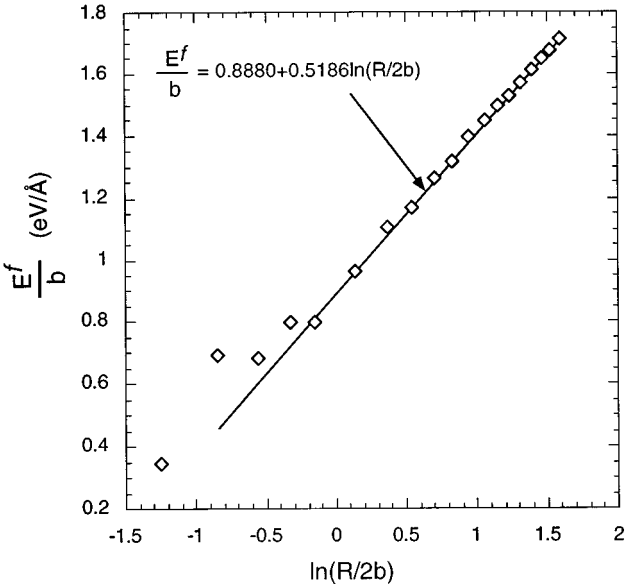

FIG. 6. Plot of E^f/b vs $\ln(R/2b)$ from the present MGPT calculations (points). The fitted MGPT points above $\ln(R/2b) = -0.144$ are shown as a solid straight line.

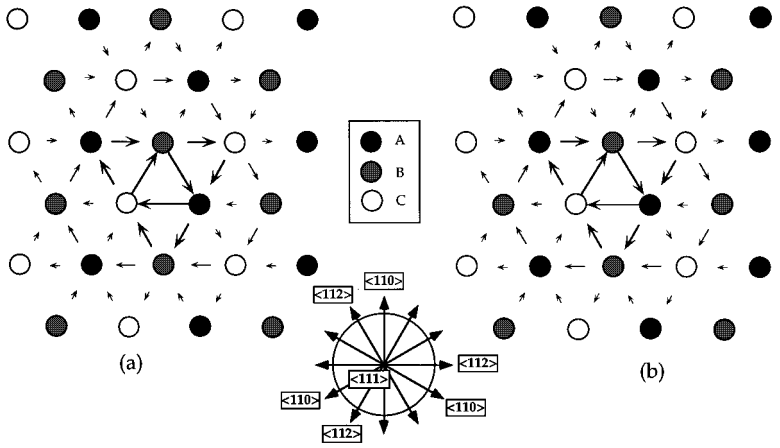

FIG. 7. The ⟨111⟩ projection of the differential displacement (DD) map of the ''hard''-core configuration from (a) anisotropic elasticity theory and (b) MGPT interatomic potentials.

displayed in Fig. 6. In this plot we find a large amount of scatter for small values of R. When $\ln(R/2b) \geqslant -0.144$, however, the data conform well to a straight line. At that point, $R = 1.73b$, which is indeed close to the assumed value of $2b$ for the core radius. The corresponding core energy E^f_{core}/b is about 0.80 eV/Å, with $b = \sqrt{3}a/2 = 2.72$ Å. By fitting those points with $\ln(R/2b) \geqslant -0.144$ to a straight line, we further infer via Eq. (14) a value of $K_s = 1.406$ Mbar from our MGPT calculations, in good agreement with the above elasticity-theory prediction.

The differential displacement (DD) method[2] has been used to elaborate the detailed characteristics of our final MGPT dislocation-core configurations. In the DD method the ⟨111⟩ component of the relative displacement of neighboring atoms due to the dislocation (i.e., the total relative displacement less than that in the perfect lattice) is drawn as an arrow between the corresponding atoms. For each atom the differential displacements of the six nearest-neighbor atoms in the ⟨111⟩ projection, corresponding to the ⟨111⟩ displacements in the three {110} planes (i.e., along three ⟨112⟩ directions), can be shown. The DD map for the MGPT ''hard''-core configuration is very similar to that generated from anisotropic elasticity theory, as shown in Fig. 7. Both results are also very similar to the nondegenerate core previously calculated by Kimura *et al.*,[32] as mentioned above. The DD map of the MGPT ''easy'' core, on the other hand, is much different than that predicted by anisotropic elasticity theory. Substantial atomic rearrangement occurs after the core region is fully relaxed. The high symmetry of the anisotropic-elastic core is broken and a threefold symmetric core which spreads out along the three ⟨112⟩ directions is obtained, as illustrated in Fig. 8. The threefold symmetry of the core extensions is reminiscent of Hirsch's early suggestion of a threefold dissociation of the core into three partial dislocations. Such a conclusion was also reached in earlier theoretical studies.[2,33]

One significant question is raised from these calculations: why does the ''easy'' ⟨111⟩ screw dislocation spread out along the ⟨112⟩ directions? A simple argument which is based on tracking the change of nearest-neighbor (NN) bond lengths and bond angles has been developed to help answer this complicated question. A detailed comparison has been made between the bond lengths and bond angles of the anisotropic-elastic dislocation core (without spread out) and the MGPT dislocation core (with spread out). For the three atoms surrounding the dislocation center, we have found that all of their NN bond lengths except one are closer to the bcc value in the MGPT core (see Table VIII). Most importantly, the NN bond angles are found to be closer to those of the bulk bcc structure when the dislocation spreads out along the three ⟨112⟩ directions (see Table IX). This is a reflection of the strong MGPT angular forces which favor the bcc bond angles. Thus it is energetically favorable for an ''easy'' ⟨111⟩ screw dislocation to be spread out in such a way as to restore the bulklike structure.

VI. CONCLUSIONS

In summary, we have systematically studied ideal shear strength, vacancy and self-interstitial formation and migra-

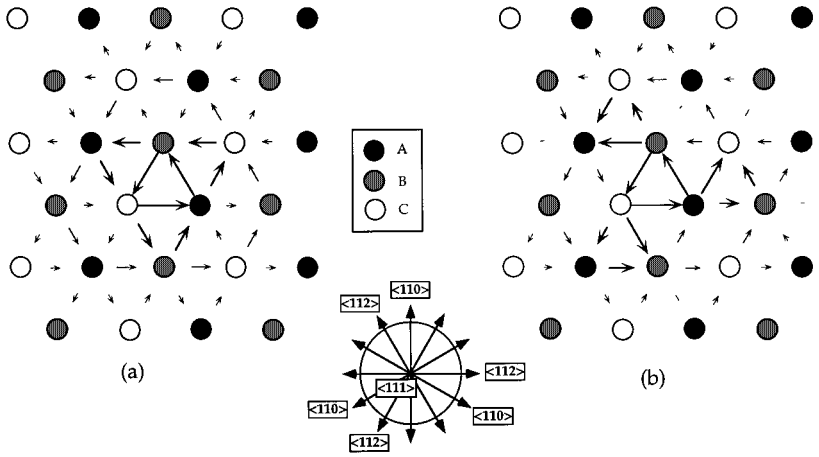

FIG. 8. The ⟨111⟩ projection of the differential displacement (DD) map of the ''easy''-core configuration from (a) anisotropic elasticity theory and (b) MGPT interatomic potentials.

TABLE VIII. Percentage difference of NN bond lengths for atoms which surrounds the dislocation center compared with a perfect bcc structure.

Anisotropic elastic theory	MGPT
−3.3%	−1.0%
−3.3%	−1.5%
−1.7%	+1.3 %
−1.7%	+1.5 %
+2.3%	+1.8%
+2.3%	+5.1%

TABLE IX. Major changes of angles between NN bonds for atoms which surrounds the dislocation.

bcc structure	Anisotropic elastic theory	MGPT
70.5	67.8	70.7
90.0	80.1	86.0
109.5	99.9	105.6 [a]
180.0	122.3	117.0 [a]

[a]Involved the spread out along ⟨112⟩ directions.

tion, and the core structure of ⟨111⟩ screw dislocations in the bcc transition metal Mo, using multi-ion MGPT interatomic potentials derived from first-principles generalized pseudopotential theory. Our calculated shear strength agrees well with previous theoretical results obtained from full electronic-structure calculations, while our calculated vacancy formation and activation energies are in excellent agreement with experimental results. The ⟨110⟩ split dumbbell interstitial is found to have the lowest formation energy, also in agreement with experiment, and with a calculated migration energy much larger than previous theoretical estimates. The atomic structures of ⟨111⟩ screw dislocations in Mo have been investigated, and it is found that the stable dislocation core structure involves spread out along the three ⟨112⟩ directions. A simple argument based on bond coordination and bond angles has been proposed to explain this spread out. In the future, we intend to extend this work to the study of dislocation mobility, including the calculation of the Peierls barrier, and to treat additional bcc metals such as tantalum.

More generally, we expect that both *ab initio* and model GPT interatomic potentials can be developed and applied to a wide variety of metallic systems and mechanical phenomena. For example, with suitable local-environment modulation,[22] MGPT potentials should be able to address the problems of fracture and crack propagation in bcc transition metals. In addition, the first-principles GPT is currently being extended to binary intermetallics, so that compounds and alloys will be treatable in the future. In this regard, *ab initio* GPT potentials for the $3d$ transition-metal aluminides are being developed as the first application of this capability.

ACKNOWLEDGMENTS

The authors wish to thank Dr. A. T. Paxton for helpful discussions on the calculation of ideal shear strength and for suggesting this application as a useful test of the MGPT potentials. This work was performed under the auspices of the U.S. Department of Energy by the Lawrence Livermore National Laboratory under Contract No. W-7405-ENG-48.

[1] For example, J. R. Rice, Mech. Mater. **6**, 317 (1987).
[2] V. Vitek, Cryst. Lattice Defects **5**, 1 (1974), and references therein.
[3] C. C. Matthai and D. J. Bacon, Philos. Mag. A **52**, 1 (1985).
[4] J. M. Harder and D. J. Bacon, Philos. Mag. A **54**, 651 (1986).
[5] R. Thetford, in *Many-Atom Interactions in Solids*, edited by R. M. Nieminen, M. J. Puska, and M. J. Manninen (Springer-Verlag, Berlin, 1990), p. 176.
[6] M. W. Finnis and J. E. Sinclair, Philos. Mag. A **50**, 45 (1984).
[7] M. S. Daw and M. I. Baskes, Phys. Rev. Lett. **50**, 1285 (1983); Phys. Rev. B **29**, 6443 (1984); S. M. Foiles, M. S. Daw, and M. I. Baskes, *ibid.* **33**, 7983 (1986).
[8] A. E. Carlsson, in *Solid State Physics: Advances in Research and Applications*, edited by H. Ehrenreich and D. Turnbull (Academic Press, Boston, 1990), Vol. **43**, p. 1.
[9] A. E. Carlsson, Phys. Rev. B **44**, 6590 (1991).
[10] D. G. Pettifor, Phys. Rev. Lett. **63**, 2480 (1989); M. Aoki, *ibid.* **71**, 3842 (1993).
[11] S. M. Foiles, Phys. Rev. B **48**, 4287 (1993).
[12] W. Xu and J. B. Adams, Surf. Sci. **301**, 371 (1994).
[13] J. A. Moriarty, Phys. Rev. B **38**, 3199 (1988).
[14] J. A. Moriarty, Phys. Rev. B **42**, 1609 (1990).
[15] J. A. Moriarty, Phys. Rev. B **49**, 12 431 (1994). A useful set of data and subroutines implementing the Mo MGPT interatomic potentials for atomistic simulation is available to the interested reader via the internet. Send e-mail requests to moriarty@sycamore.llnl.gov .
[16] C. Kittel, *Introduction to Solid State Physics*, 5th ed. (Wiley, New York, 1976), p. 74.
[17] D. L. Davidson and F. R. Brotzen, J. Appl. Phys. **39**, 5768 (1968).
[18] B. M. Powell, P. Martel, and A. D. B. Woods, Can. J. Phys. **55**, 1601 (1977).
[19] M. Alouani, R. C. Albers, and M. Methfessel, Phys. Rev. B **43**, 6500 (1991).
[20] K.-M. Ho, C.-L. Fu, and B. N. Harmon, Phys. Rev. B **29**, 1575 (1984).
[21] Y. Chen, C.-L. Fu, K.-M. Ho, and B. N. Harmon, Phys. Rev. B **31**, 6775 (1985).
[22] J. A. Moriarty and R. Phillips, Phys. Rev. Lett. **66**, 3036 (1991).
[23] A. T. Paxton, P. Gumbsch, and M. Methfessel, Philos. Mag. Lett. **63**, 267 (1991).
[24] J. D. Althoff, P. B. Allen, R. M. Wentzcovitch, and J. A. Moriarty, Phys. Rev. B **48**, 13 253 (1993); J. A. Moriarty and J. D. Althoff, *ibid.* **51**, 5609 (1995).
[25] J. A. Moriarty (unpublished).
[26] W. H. Press, B. P. Flannery, S. A. Teukolsky, and W. T. Vetterling, *Numerical Recipes in Fortran* (Cambridge University Press, Cambridge, 1992).
[27] K. Maier, M. Peo, B. Saile, H. E. Schaefer, and A. Seeger, Philos. Mag. A **40**, 701 (1979).

[28] Y. Ohta, M. W. Finnis, D. G. Pettifor, and A. P. Sutton, J. Phys. F **17**, L273 (1987).
[29] P. Erhart, J. Nucl. Mater. **69**, 200 (1978).
[30] R. Thetford, Harwell Report No. AERE M3507 (HMSO, London, 1985); G. J. Ackland and R. Thetford, Philos. Mag. A **56**, 15 (1987).
[31] J. D. Eshelby, W. T. Read, and W. Shockley, Acta Metall. **1**, 251 (1953); A. N. Stroh, Philos. Mag. **3**, 625 (1958); A. K. Head, Phys. Status Solidi **6**, 461 (1964); J. P. Hirth and J. Lothe, *ibid.* **15**, 487 (1966); Y. T. Chou and T. E. Mitchell, J. Appl. Phys. **38**, 1535 (1967).
[32] K. Kimura, S. Takeuchi, and K. Masuda-Jindo, Philos. Mag. A **60**, 667 (1989).
[33] M. S. Duesbury, Contemp. Phys. **27**, 145 (1986).